REYNOLDS-STRESS MODELING OF AFTERBODY FLOWS

Paul Batten,
Metacomp Technologies Inc, 650 Hampshire Rd #200,
Westlake Village, CA 91361, USA,

Michael A. Leschziner, Tim J. Craft,
Dept. of Mechanical Engineering, UMIST,
Sackville St, Manchester, UK

ABSTRACT

Several afterbody flows involving shock/boundary-layer interaction, and representative of conditions at the rear of high-speed aircraft, are used to evaluate a new form of a realizable low-Reynolds-number second-moment turbulence closure. The model considered is a variant of the closure of Craft and Launder (1996), which includes a tensorially cubic model for the pressure-strain, ϕ_{ij}, and which is directly applicable to low-Reynolds number flows without the use of surface-topography parameters, such as wall-normal distance. New features associated with the extension of the model to compressible flow are outlined, and improved predictions are reported for several applications, relative to results arising from low-Reynolds-number k-ϵ and 'linear' variants of second-moment-closure.

INTRODUCTION

There are a number of important aerospace applications in which turbulent boundary layers developing on a streamlined body interact with and strongly modify inviscid flow features associated with shock waves. Such an interaction may occur over wings in transonic or supersonic flight and on the curved exterior 'boattail' surface of high-pressure exhaust systems, the latter contributing up to 30% of the total aircraft drag. If the localized region of adverse-pressure gradient generated by the shock wave is sufficiently strong, the turbulent boundary layer will separate, drastically affecting the primary operational characteristics of the body, specifically its lift and drag.

The superiority of anisotropy-resolving non-linear eddy-viscosity and second-moment turbulence models in predicting shock/boundary-layer interaction has been demonstrated by, amongst others, Benay et al. (1987), Lien and Leschziner (1993) and Loyau et al. (1998). Although highly-tuned isotropic models can give equally good predictions in many of these flows, the more elaborate models offer the potential of greater generality and applicability over a broader range of conditions and tend to resolve local small-scale features which isotropic eddy-viscosity models fail to capture.

Recent work by Batten et al. (1999) has focused on the development and validation of a new variant of realizable, low-Re-number, 'cubic' second-moment closure, based on that of Craft and Launder (1996), with particular emphasis placed on shock-affected boundary layers. This paper reports results arising from an investigation of the new model for compressible flow over several afterbody configurations.

THE TURBULENCE CLOSURE

The present closure originated from the cubic pressure-strain model developed initially for incompressible turbulent flow by Fu (1988), and later extended to low Reynolds-number conditions by Launder and Tselepidakis (1993), Launder and Li (1994) and Craft and Launder (1996). The present variant includes recent refinements proposed by Craft (1998) and Iacovides and Raisee (1997). The principal developments conveyed here relate to the response of the model to shock-containing regions, especially where the shock interacts strongly with a boundary layer, to the extent of provoking separation. The functional dependence of the low-Reynolds-number model of Craft and Launder (1996) on the anisotropy invariants was found to misrepresent the response of turbulence to shock waves. Specifically, the combination of length-scale and anisotropy-sensitized coefficients of the model was observed to cause turbulence to approach the two-component limit at shocks, from which the flow failed to recover after passing through the shock. New functional relations are considered which remove this unphysical behaviour, yet maintain all the original advantageous model properties for incompressible flow. This

is first verified by reference to homogeneous flow and incompressible impinging-jet flow. The performance of the modified model is then demonstrated over a range of afterbody configurations involving strong shock/boundary-layer interaction.

The mass-averaged Reynolds-stress-transport equations are first written in the form:

$$\frac{\partial \overline{\rho}\widetilde{u_i''u_j''}}{\partial t} + \frac{\partial \overline{\rho}\widetilde{u_i''u_j''}\widetilde{u}_k}{\partial x_k} = P_{ij} + d_{ij} + \phi^*_{ij} - \epsilon_{ij}$$

in which the production terms, P_{ij}, are exact and require no modeling. The diffusion terms, d_{ij}, are modeled using a combination of the GGDH (Daly & Harlow) and a pressure-diffusion model proposed by Craft and Launder (1996). Both the pressure-diffusion and the pressure-strain (ϕ^*_{ij}) models incorporate dimensionless gradient indicators, which vanish in regions of weak inhomogeneity, but behave essentially as unit 'normal-to-wall' vectors in the presence of large gradients of turbulence length scale. The gradient indicators take the form:

$$d_i^A = N_i^A/[0.5 + \sqrt{N_k^A N_k^A}] \quad \text{with} \quad N_i^A = \frac{\partial(l\sqrt{A})}{\partial x_i}$$

in which $A = 1 - 9/8(a_{ij}a_{ij} - a_{ij}a_{jk}a_{ki})$ is Lumley's stress-flatness parameter and $l = \widetilde{k}^{\frac{3}{2}}/\widetilde{\epsilon}$ is the turbulence length-scale. The pressure-strain correlation, ϕ^*_{ij}, is considered as a sum of slow, rapid and inhomogeneity correction terms:

$$\phi^*_{ij} = \phi^*_{ij1} + \phi^*_{ij2} + \phi^{inh}_{ij}$$

in which the corrections, ϕ^{inh}_{ij}, take the form:

$$\phi^{inh}_{ij} = f_w \frac{\overline{\rho}\widetilde{\epsilon}}{\widetilde{k}}(\widetilde{u_l''u_k''}d_l^A d_k^A\delta_{ij} - \frac{3}{2}\widetilde{u_i''u_k''}d_j^A d_k^A - \frac{3}{2}\widetilde{u_j''u_k''}d_i^A d_k^A)$$

and the damping function, f_w is taken as:

$$f_w = \beta(1 - A^{\frac{1}{2}})\min[1, \max(0, 1 - (R_t - 55)/70)]$$

with $R_t = \widetilde{k}^2/\widetilde{\nu\epsilon}$, the turbulent Reynolds number. The above functional form ensures that the corrections are active only in regions in which strong inhomogeneity occurs in combination with small values of turbulence Reynolds number and near-zero stress-flatness parameter - i.e., in the immediate vicinity of a solid surface.

The dissipation tensor, ϵ_{ij} is modeled as:

$$\epsilon_{ij} = (1 - A^{\frac{1}{2}})\overline{\rho}(\epsilon'_{ij} + \epsilon''_{ij})/D + 2/3A^{\frac{1}{2}}\overline{\rho}\widetilde{\epsilon}\delta_{ij},$$

with $D = (\epsilon'_{kk} + \epsilon''_{kk})/(2\widetilde{\epsilon})$. This causes ϵ_{ij} to blend from isotropic to a near-wall limiting dissipation, with an additional modification, ϵ''_{ij}, designed to mimic an observed dip in the shear-stress dissipation rate in the buffer layer.

An equation for the homogeneous dissipation rate is adopted:

$$\frac{\partial \overline{\rho}\widetilde{\epsilon^*}}{\partial t} + \frac{\partial \overline{\rho}\widetilde{\epsilon^*}\widetilde{u}_k}{\partial x_k} = \frac{\partial}{\partial x_l}\left[\left(\widetilde{\mu}\delta_{lk} + C_\epsilon \overline{\rho}\widetilde{u_l''u_k''}\frac{\widetilde{k}}{\widetilde{\epsilon}}\right)\frac{\partial \widetilde{\epsilon^*}}{\partial x_k}\right] + \frac{C_{\epsilon 1}\overline{\rho}P_k}{\tau} - \frac{C_{\epsilon 2}\overline{\rho}\widetilde{\epsilon^*}}{\tau} - \frac{C_{\epsilon 3}(\widetilde{\epsilon} - \widetilde{\epsilon^*})\overline{\rho}\widetilde{\epsilon^*}}{\widetilde{k}} + C_{\epsilon 4}\widetilde{\mu}\tau\widetilde{u_i''u_j''}\frac{\partial^2\widetilde{u}_k}{\partial x_i \partial x_l}\frac{\partial^2\widetilde{u}_k}{\partial x_j \partial x_l} + \frac{C_{\epsilon 5}\overline{\rho}\widetilde{\epsilon^*}}{\tau}Y_P$$

in which

$$Y_P = 0.2\min\left\{\max\left[F(F+1)^2, 0\right], 20\right\}$$

$$F = \left[\sqrt{\left(\frac{\partial l}{\partial x_j}\right)\left(\frac{\partial l}{\partial x_j}\right)} - \frac{\partial l_e}{\partial Y}\right]/c_l$$

$$\frac{\partial l_e}{\partial Y} = c_l\left[1 - \exp(-B_\epsilon R_t) + B_\epsilon R_t \exp(-B_\epsilon R_t)\right]$$

$$c_l = 2.55, \quad B_\epsilon = 0.1069, \quad \tau = \frac{\widetilde{k}}{\widetilde{\epsilon}}$$

$$C_{\epsilon 1} = 1.44, \quad C_{\epsilon 2} = 1.92, \quad C_{\epsilon 3} = 1.0, \quad C_{\epsilon 4} = 0.4,$$

$$C_{\epsilon 5} = 0.2, \quad C_\epsilon = 0.18$$

Finally, the turbulent heat-flux terms appearing in the mean energy equation are modeled using a thin-layer form of the GGDH:

$$-\overline{\rho}\widetilde{T''u_i''}n_i = c_\theta \frac{\overline{\rho}\widetilde{k}}{\widetilde{\epsilon}}\widetilde{u_i''u_k''}n_i n_k n_j \frac{\partial \widetilde{T}}{\partial \widetilde{x_j}}.$$

Full details of the model are given in Batten et al. (1999).

RESULTS

In the following sub-sections, a series of test flows of increasing complexity are presented. The model's performance is first demonstrated by reference to homogeneous flow and incompressible impinging jet flow. Results are then presented for compressible axisymmetric afterbody flows with solid stings 'simulating' the afterbody jet, then with jet regions at high nozzle-pressure ratios, and finally for a fully three-dimensional afterbody configuration.

Computations were performed using an implicit scheme based on the HLLC approximate Riemann solver (Batten et al. , 1997). The axi-symmetric configurations were all computed with 3D grids, generated by rotating a 2D mesh through $\pm 10^{-2}$ Radians and then considering the azimuthal planes of the segment to be symmetry planes. Boundary conditions relating to these planes were imposed for each Reynolds-stress equation, with the 'rotated' Reynolds-stress values established by taking products of rotated velocity fluctuations. For each stress equation, semi-implicit relations were established for these boundary stresses, as well as for all source and deferred correction terms in order to maximize under-relaxation and ensure positivity of the normal stresses.

Homogeneous Flow

The first two examples are for homogeneous turbulence perturbed by invariant axi-symmetric contraction and expansion, respectively. Fig. 1 shows comparisons of results computed with the present model (MCL) and that of Jakirlić-Hanjalić (1995) (JH), the latter using the linear 'isotropisation of production' (IP) pressure-strain approximation, against DNS data of Lee and Reynolds (1985). The stress components are plotted against $t' = S^*t$, with $S^* = (k/\epsilon)\sqrt{S_{ij}S_{ij}/2}$ corresponding to the mean strain-rate parameter. Linear eddy-viscosity models seriously mis-represent the normal stresses and are not included.

Impinging-Jet Flow

This flow is a low-speed, round air jet which discharges from a smooth pipe and impinges normally on a flat plate. The jet was discharged at the height, $H = 2D$, and the Reynolds number was 23,000, based on bulk velocity and internal pipe diameter, D. The jet-exit conditions were first determined from a fully-developed pipe-flow calculation. A 121×121 grid, known to support grid-independent solutions with the present numerical method, was used, with 51 points across the jet radius and an outflow side boundary which extended 8 jet diameters from the pipe centerline. Reservoir conditions, corresponding to constant stagnation temperature and pressure, were imposed at the entrainment boundary adjacent to the pipe. Fig. 2 presents profiles of axial normal stresses along the stagnation line and mean-velocity profiles at $R=D$, in comparison with the experimental measurements of Cooper et al. (1993). The most noticeable discrepancies occur in the stagnation region, where the linear eddy-viscosity (k-ϵ and SST) models show a massive over-prediction of k and hence of all normal stresses. The Jakirlić-Hanjalić (1995) (JH) Reynolds-stress model gives only a modest improvement over the k-ϵ model. This is due, in part, to known weaknesses with the conventional wall-reflection terms used in this model (see, for example, Craft and Launder (1992).

Langley Afterbodies

Three afterbody configurations have been investigated experimentally at NASA Langley to test the feasibility of measuring afterbody drag without having to plumb the model interior to simulate a jet exhaust. These configurations comprised solid metal 'plumes' (or stings) in their base regions to simulate the blocking effect of the jet on the outer flow. The results presented here correspond to the first of the three configurations at both subsonic ($M=0.8$) and supersonic ($M=1.2$) conditions. A compressible Musker formulation was used to impose an incoming boundary layer of thickness of $0.18D$, with D the (exterior) diameter of the afterbody.

Boattail pressure distributions in Fig. 3 demonstrate the improved flow representation obtained with the present model relative to that returned by the k-ϵ and the Jakirlić-Hanjalić models. For this case, the SST model (Menter, 1994), gives agreement comparable to that of the present Reynolds-stress model, but owing to quite a different modeling mechanism.

Carson & Lee Afterbodies

A wide range of afterbody geometries and flow conditions have been considered experimentally by Carson and Lee (1981). This series of tests were designed to cover a range of flight-like conditions, from subsonic acceleration through to supersonic cruise. The high jet-pressure ratios and boattail curvatures examined in cases 1 and 4 (Carson & Lee, 1981) resulted in substantial shock-induced separation of the flow from the boattail region of the afterbody, and these cases are therefore of principal interest herein.

An exterior boundary-layer thickness of $0.1D$ was assumed for both cases, with D the internal nozzle diameter. Reservoir conditions corresponding to $k=10^{-4}u_\infty^2$ and $\mu_t=10^{-4}\mu$ were prescribed at the jet-exit boundary. The agreement shown in Figs. 4 and 5 is good for the interior throat section of both nozzles, suggesting the interior jet flow is essentially governed by inviscid processes. Agreement for the boattail pressure coefficient is variable, with the SST and present models correctly predicting a more extensive separation-related pressure plateau.

AGARD-A1 Afterbody

For this test case, there are more extensive experimental data available, including velocity and total pressure distributions across the jet (see for example, Newbold (1990) and Peace (1991)). Results are presented here for Case 5, which features a free-stream flow at Mach 0.7, a jet condition corresponding to a nozzle-pressure ratio (jet-total/free-stream pressure) of 3.0 and an incoming boundary-layer thickness of $0.1D$, with D being the maximum interior nozzle diameter.

Figs. 6,7, show results computed with jet conditions corresponding to a total temperature of 300K, a turbulence intensity of $10^{-2}u_\infty^2$ and a dissipation rate specified from $\mu_t=10^2\mu$. The rapid erosion of the jet's shock-cell structure is primarily due to the high turbulence levels in the jet. All predictions show good agreement in respect of the boattail pressure levels, with the exception of the Jakirlić-Hanjalić model, which appears to predict a relaminarisation of the flow before the end of the boattail, resulting in a severe underestimation of the jet- spreading rate downstream. The SST results are closely similar to those returned by the Launder-Sharma k-ϵ model. This is expected, because the SST model is, in effect, a linear k-ϵ model away from walls.

Test calculations have revealed a significant sensitivity of the jet structure to the imposed levels of turbulence at the jet-exit boundary was observed. Peace (1991) has previously reported a pronounced underestimation of the jet spreading rate and suggested that this reflected turbulence-model defects. However, we have observed that low levels of eddy viscosity at the jet-exit boundary ($\mu_t \leq \mu$) also cause a significant underestimation of the shear-layer thickness at the measured locations downstream of the jet exit. This poses a question mark against the jet-exit boundary conditions used for these cases. The discrepancy in the velocity profiles at the boattail edge, ($x/Dm = 0$) predicted by all models, is probably also related to uncertainties in the experimental jet conditions, perhaps specifically associated with an under-developed boundary layer on the inner surface of the nozzle.

AGARD-B2 Afterbody

This case is a configuration from a range of single-engine-fighter models tested in the NASA Langley 16-

foot transonic wind tunnel (Berrier, 1988). The aim of these tests was to examine tail-interference effects on an otherwise axi-symmetric afterbody. The case considered here is that of $M_\infty = 0.944$ with a nozzle-pressure ratio of $p_{T,j}/p_\infty = 1.98$. The flow was impulsively started from free-stream conditions, with reservoir conditions specified at the jet-exit boundary corresponding to a total temperature of 302K and a total pressure of $1.98p_\infty$. Turbulence levels in the jet were specified from $k = u_\infty^2 \times 10^{-4}$ and $\mu_t = \mu$. The turbulence levels in the free-stream were similarly specified, although ϵ_∞ was determined from $\mu_t = 10\mu$, with all turbulence source terms set to zero ahead of the leading edge of the model at $x = 0$. Calculations were performed with an 831-block mesh containing around 1.4 million nodes.

Large diffusivities in the wake arise here in combination with highly stretched grids at mesh-block interfaces, which results in a slow transfer of information across zones near the edge of the jet. This proved to be especially problematic in conjunction with linear k-ϵ models. The present Reynolds-stress model proved more stable, but it was still necessary to keep the local CFL number at around 10 (all other cases reported here ran at a local CFL of order 1000). Fig. 8 shows results for the boattail-surface pressure obtained with the present model, which agree closely with the very limited amount of experimental data available.

CONCLUSIONS

This paper has considered the application of a new generation of low-Reynolds number Reynolds-stress transport model to a range of afterbody configurations featuring shock/boundary-layer interaction. Consistent improvements are observed relative to *conventional* linear k-ϵ models. The recently refined low-Reynolds number *linear* Reynolds-Stress model of Jakirlić-Hanjalić (JH) shows some modest improvement over the linear k-ϵ model, but was found to significantly under-predict the spread of the jet-shear layer in the AGARD-A1 case. The present model yields predictions which are at least as good as, and in most cases significantly better than, those returned by the JH model which incorporates the conventional Gibson and Launder (1987) wall corrections. Although Menter's two-equation (SST) formulation (Menter, 1994) gives results comparable to those of the present model for jet-afterbody flows, its generality is substantially narrower, as was illustrated by reference to the impinging jet. This also applies to other highly tuned eddy-viscosity models.

As experimental data for many cases examined is strictly limited, and usually confined to wall pressure, definitive conclusions are difficult to draw. Differences between predictions and experiments arise especially in cases with strong jet-pressure ratios or highly curved boattails (both of which tend to provoke separation). However, there are significant uncertainties in relation to the realism of the boundary conditions, especially at the jet exit.

ACKNOWLEDGMENTS

The financial support of British Aerospace and the Royal Society of London is gratefully acknowledged. The authors would also like to thank Keith Weatherill of BAe, Warton, for supplying the AGARD-B2 multi-block mesh.

REFERENCES

P. Batten, T.J. Craft, M.A. Leschziner, and H. Loyau, 1999, To appear in AIAA.

P. Batten, M.A. Leschziner, and U. C. Goldberg, 1997, *JCP*, 137:38–78.

R. Benay, M.C. Coët, and J. Délery, 1987, In *6th Turbulent Shear Flow Symposium, Toulouse, France*, pages 8.2.1–8.2.6.

B.L. Berrier, 1988, Technical report, AGARD-AR-303, Vol 2 - A Selection of Experimental Test Cases for the Validation of CFD Codes.

G.T. Carson Jr. and E.E. Lee Jr, 1981, Technical report, NASA TP 1953.

D. Cooper, D.C. Jackson, B.E. Launder, and G.X. Liao, 1993, *International Journal of Heat and Mass Transfer*, 36:2675–2684.

T.J. Craft, 1998, *Int. J. Heat and Fluid Flow*, 19:541–548.

T.J. Craft and B.E. Launder, 1992, *AIAA*, 30(12):2970–2972.

T.J. Craft and B.E. Launder, 1996, *Int. J. Heat and Fluid Flow*, 17:245–254.

S. Fu, 1988, Ph.D. Thesis, Dept. of Mechanical Engineering, UMIST.

M.M. Gibson and B.E. Launder, 1987, *J. Fluid. Mech.*, 86(3):491–511.

H. Iacovides and M. Raisee, 1997, In *2nd International Symposium on Turbulence, Heat and Mass Transfer, K. Hanjalic and T. W. J. Peters (Eds.)*.

S. Jakirlic and K. Hanjalic, 1995, In *10th Symposium on Turbulent Shear Flows, Pensilvania State University*, volume 3.

B.E. Launder and S-P. Li, 1994, *Physics of Fluids*, 6:999–1006.

B.E. Launder and B.I. Sharma, 1974, *Letters in Heat and Mass Transfer*, 1:131–138.

B.E. Launder and D.P. Tselepidakis, 1993, In *Turbulent Shear Flow*, volume 8. Springer.

M.J. Lee and W.C. Reynolds, 1985, Technical report, Report TF-24, Department of Mechanical Engineering, Stanford University.

F.S. Lien and M.A. Leschziner, 1993, *Journal of Fluids Engineering*, 115.

H. Loyau, P. Batten, and M.A. Leschziner, 1999, *ERCOFTAC Journal of Flow, Turbulence and Combustion*, 60(3):257-282.

F.R. Menter, 1994, *AIAA*, 32(8).

C.M. Newbold, 1990, Technical report, ARA TN 90-16 (Unpublished).

A.J. Peace, 1991, *Journal of Propulsion and Power*, 7(3).

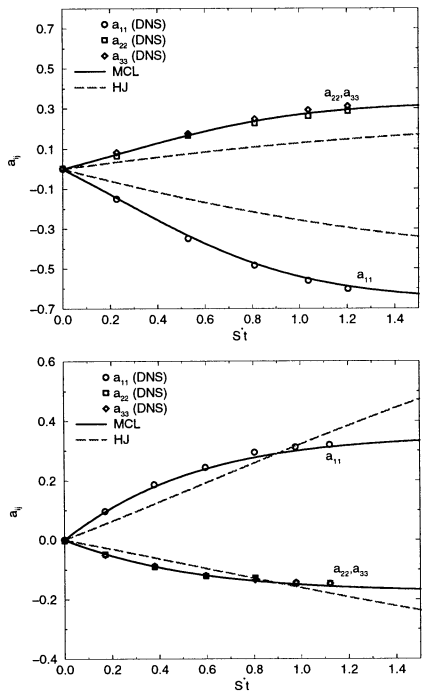

Figure 1: Homogeneous axisymmetric contraction (upper) and expansion (lower)

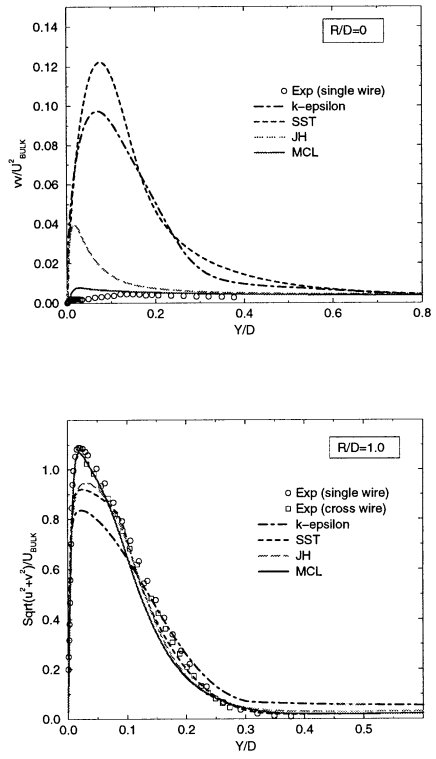

Figure 2: Impinging jet - $\widetilde{v'v'}$ on stagnation line (upper) and mean velocity at $R = D$ (lower)

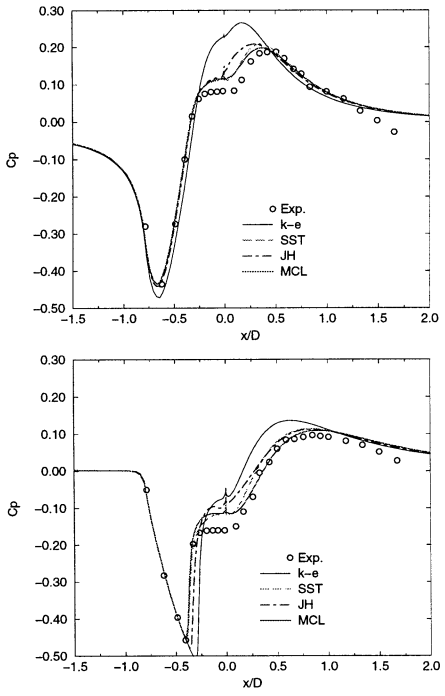

Figure 3: Langley configuration 1, $M_\infty = 0.8$ (upper) and $M_\infty = 1.2$ (lower)

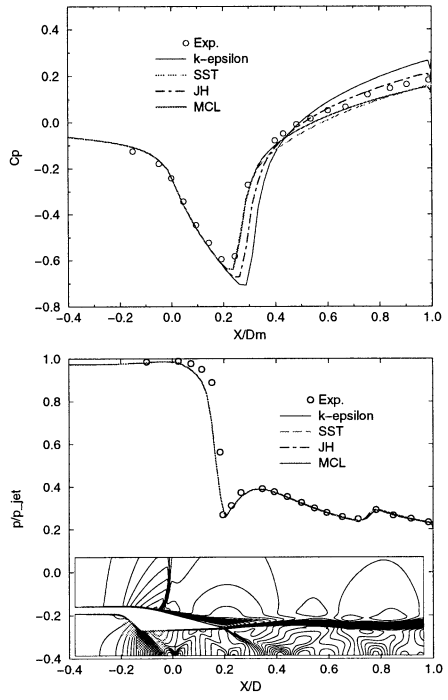

Figure 4: Carson and Lee configuration 1 - Iso-Mach contours, boattail Cp and internal nozzle p/p_{jet}^T)

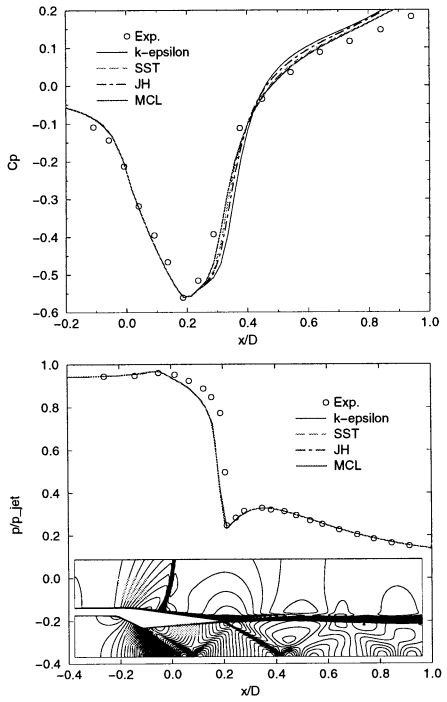

Figure 5: Carson and Lee configuration 4 - IsoMach contours, boattail Cp and internal nozzle p/p^T_{jet}

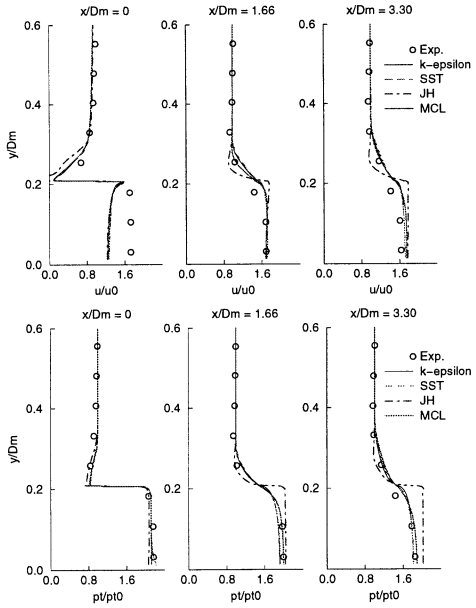

Figure 6: AGARD-A1 - Velocity & total pressure distributions across jet

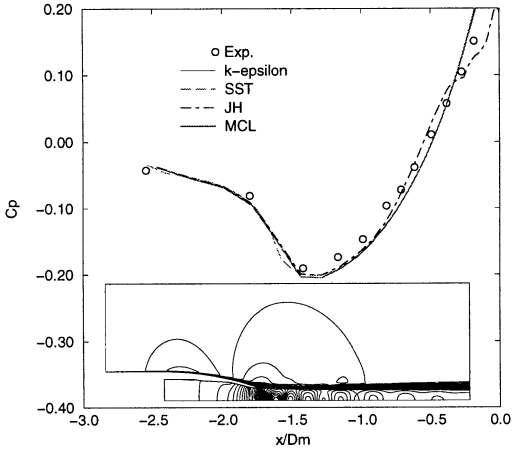

Figure 7: AGARD-A1 - IsoMach contours & boat-tail Cp distributions

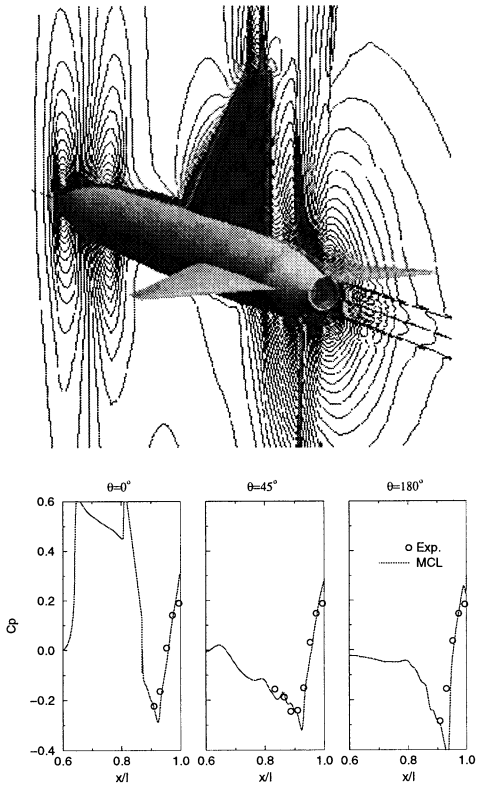

Figure 8: AGARD-B2 - Isobar contours & boattail pressure distributions